Journal of The Electrochemical Society, **152** (1) G83-G91 (2005)
0013-4651/2004/152(1)/G83/9/$7.00 © The Electrochemical Society, Inc.

Numerical and Experimental Analysis of Cu Diffusion in Plasma-Treated Tungsten Barrier

Kou-Chiang Tsai,[a] Wen-Fa Wu,[b,*,z] Jen-Chung Chen,[a] Te-Jen Pan,[a] and Chuen-Guang Chao[a]

[a]*Department of Materials Science and Engineering, National Chiao Tung University, Hsinchu 300, Taiwan*
[b]*National Nano Device Laboratories, Hsinchu 300, Taiwan*

This work investigates Cu diffusion in sputtered and N_2O plasma-treated W films. N_2O plasma-treated W barrier has a nanostructured surface layer and shows high thermal stability and the best barrier properties. Also investigated herein are the lattice and grain boundary diffusivities extracted from the Cu penetration depth profiles using the Whipple analysis of grain boundary diffusion and Fick's second law of diffusion. Analysis indicates that the diffusion models correlate well with experimental results.
© 2004 The Electrochemical Society. [DOI: 10.1149/1.1833631] All rights reserved.

Manuscript submitted March 22, 2004; revised manuscript received June 10, 2004. Available electronically December 1, 2004.

As device dimensions decrease toward 180 nm and below, the necessity for interconnections with resistivity as low as possible is pressing. Copper is now being used in advanced metallization technology due to its low resistivity and high electromigration and stress migration resistance. However, Cu can diffuse into and react with Si or dielectric materials during annealing, and create deep trap levels that cause degradation of device performance and reliability.[1,2] Therefore, a qualified diffusion barrier inserted between Cu and Si or dielectric materials is necessary for the Cu metallization. Refractory metals and their nitrides are used as diffusion barriers in copper metallization.[3-6] Among these materials, tungsten nitride (WN) has received the most attention owing to its high thermal stability and excellent chemical mechanical polishing (CMP) process compatibility.[7] However, resistivity of tungsten nitride film is higher than that of tungsten film. As the technology node moves to 130 nm and below, a barrier layer with low resistivity is necessary to lower the resistance of the total line interconnect and/or via.

Most refractory metal films used as diffusion barriers in Cu metallization are polycrystalline rather than monocrystalline. Moreover, columnar grain structure is frequently found in sputtered refractory metal and metal nitride films.[8-10] In general, atomic diffusion along grain boundaries is much faster than in the bulk of grains. Grain boundaries may presumably serve as fast diffusion paths for copper. Coupled lattice and grain boundary diffusion is different from lattice diffusion. Whipple had given formulas for the concentration in a semi-infinite region of low diffusion coefficient bisected by a thin well-diffusing slab.[11,12] This is of interest in grain boundary diffusion.

In this study, a method of forming nitrogen and oxygen incorporated W films with low resistivity was investigated. N_2O plasma was used to post-treat the W diffusion barrier. The effectiveness of as-deposited and N_2O plasma treated W films as diffusion barriers between Cu and Si was evaluated. A composite diffusion barrier was formed after N_2O plasma treatment. Cu diffusion in the N_2O plasma treated W barrier was further analyzed by numerical calculation using Whipple's and Fick's models.

Experimental

Single crystal, (100) orientated silicon wafers were used in this study. Tungsten films of 50 nm were deposited at a power of 1000 W by sputtering. Films were sputtered at room temperature without intentional heating and base pressure was less than 6×10^{-7} Torr. The wafers further received N_2O plasma treatment in a plasma-enhanced chemical vapor deposition (PECVD) system after W films were deposited. The power and pressure of N_2O plasma treatment were 200 W and 100 mTorr, respectively. Some wafers were treated by N_2 or NH_3 plasma for comparison. For easy identification, the untreated, N_2O, N_2, and NH_3 plasma-treated W films were denoted as W, W(N_2O), W(N_2), and W(NH_3) barriers in the work. Copper films, 300 nm thick, were deposited on top of the barrier layers by sputtering. The efficiency of the diffusion barrier was analyzed by the variation of sheet resistance and leakage current densities of junction diodes after thermal stressing in N_2 ambient at 500–700°C, *i.e.*, 773–973 K, for 30 min. The wafers were administered a local oxidation of silicon (LOCOS) process to define active regions. The active regions were implanted with 5×10^{15} As^+ ions/cm^2 at energy of 60 keV for n^+-p junction diodes, and dopants were activated by rapid thermal annealing (RTA) in N_2 ambient at 1050°C for 30 s. Leakage currents of diodes were measured at a reverse bias of 5 V by a HP 4156 semiconductor parameter analyzer. A four-point probe system was employed to measure sheet resistance.

Film thickness was measured by a stylus surface profiler and scanning electron microscopy (SEM). X-ray photoemission spectroscopy (XPS) was used to study the bonding structures and chemical binding energies. The microstructure and grain size of the film were examined using transmission electron microscopy (TEM). Structure and crystalline orientation of as-deposited and annealed samples were analyzed by an X-ray diffractometer (XRD) with Cu Kα radiation operated at 50 kV and 250 mA. Surface roughness and morphology of the film were observed using a Digital Instruments Nanoscope II model atomic microscope (AFM) with a 0.5 Hz scanning speed in air ambient. Surface morphology was studied by a field-emission scanning electron microscope (FESEM). Compositional depth profiles were measured by secondary ion mass spectrometry (SIMS).

Results and Discussion

To investigate the effects of N_2O plasma treatment on W barrier, chemical bonding states of barrier were analyzed by XPS. Figure 1a-c show the W 4f, O 1s, and N 1s spectra of as-deposited and N_2O plasma-treated W barriers. The W $4f_{7/2}$ and W $4f_{5/2}$ peaks are situated at the same position (31.2, 33.4 eV) for two barriers, and the two peaks are characteristics of the W itself.[13] However, two other peaks at binding energies 36.2 and 38.4 eV are observed for the W(N_2O) barrier. The peaks correspond to binding energies of tungsten oxide and are attributed to oxidation during N_2O plasma treatment. The O 1s spectrum of the W(N_2O) barrier exhibits a strong and broad peak centered at around 531.2 eV, as shown in Fig. 1b. There is almost no peak in untreated W barrier. W-O phases are believed to form at the surface of W(N_2O) barrier. The N 1s peak of the W(N_2O) barrier can be well resolved into two peaks by curve fitting compared to no peak in the N 1s spectrum of the W barrier, as shown in Fig. 1c. These two peaks are centered at 397.5 and 399.3 eV. The weak peak centered at 397.5 eV is consistent with the N 1s binding energy of nitride compound and is also reported by previous research.[14] Another strong peak at ~399.3 eV is observed in N 1s

* Electrochemical Society Active Member.
z E-mail: wfwu@mail.ndl.org.tw

Downloaded on 2014-04-26 to IP 140.113.38.11 address. Redistribution subject to ECS terms of use (see ecsdl.org/site/terms_use) unless CC License in place (see abstract).

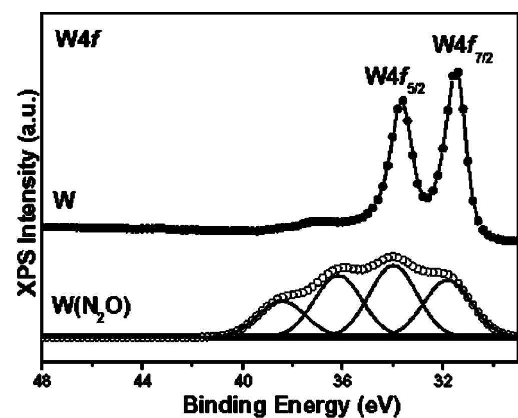

(a)

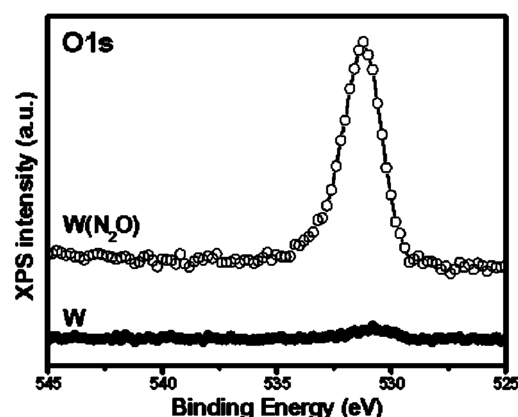

(b)

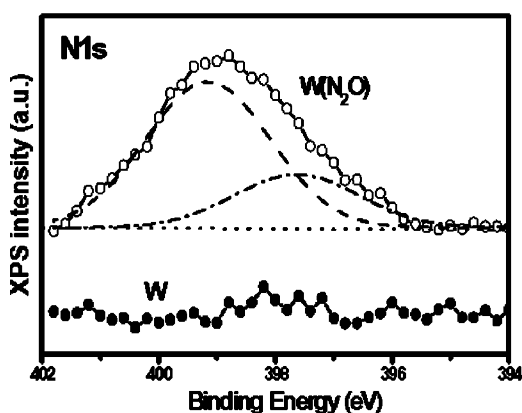

(c)

Figure 1. (a) W 4f, (b) O 1s, and (c) N 1s XPS spectra of W and $W(N_2O)$ barriers.

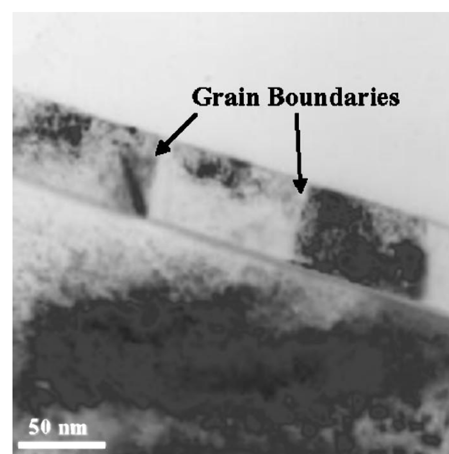

(a)

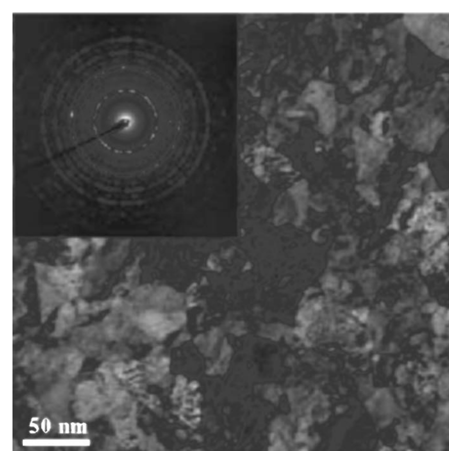

(b)

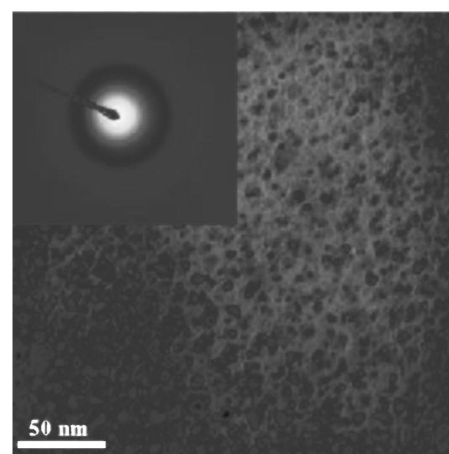

(c)

Figure 2. (a) Cross-sectional bight field TEM image of W barrier. Plane-view TEM images and SAD patterns of the (b) W and (c) $W(N_2O)$ barriers.

spectrum. This indicates that some N atoms do not form strong covalent or ionic bonds with W during N_2O plasma treatment. Some N atoms or molecules may present in grain boundaries of W.[8,15,16]

Figure 2a displays cross-sectional bright field TEM micrograph of as-sputtered W film. Columnar grain structure is observed. Cu diffusion in columnar grains is believed to be relatively easy because columnar grains will provide fast diffusion paths for Cu diffusion. Figure 2b and c display plane-view TEM images and selected area diffraction (SAD) patterns of W and $W(N_2O)$ barriers. Several sharp rings are observed for untreated W film. This indicates that the as-deposited W film is a polycrystalline structure. The grain size of as-deposited W film is 20–40 nm, as shown in Fig. 2b. The $W(N_2O)$ barrier has a diffused ring pattern instead of diffraction spots, indicating that the N_2O plasma treatment causes an amor-

Downloaded on 2014-04-26 to IP 140.113.38.11 address. Redistribution subject to ECS terms of use (see ecsdl.org/site/terms_use) unless CC License in place (see abstract).

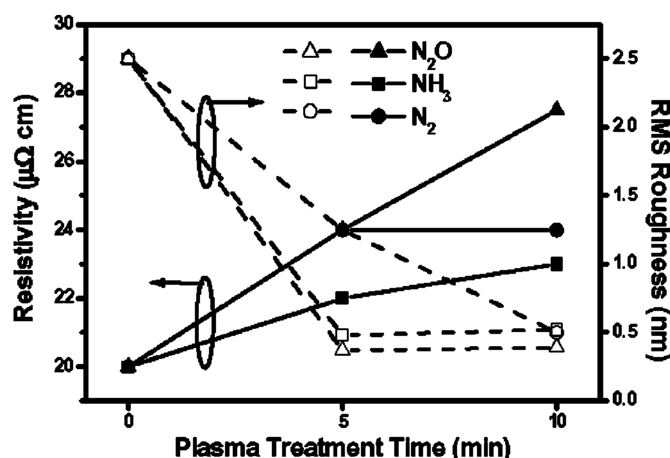

Figure 3. Resistivity and RMS surface roughness of $W(N_2)$, $W(NH_3)$, and $W(N_2O)$ films as a function of plasma treatment time.

phous surface layer upon W film. Grain size of the $W(N_2O)$ barrier is only 2–5 nm. This indicates that a surface layer with finer grains is formed due to the reactions and bombardments of energetic radicals and ions during plasma treatment. It is reported that the nanostructured amorphous diffusion barrier, defined as a very short-range order single crystal, is highly attractive due to its relatively high thermal stability and its relatively higher resistance against Cu diffusion.[17]

Figure 3 displays resistivity and root-mean-square (RMS) surface roughness of plasma treated W film as a function of plasma treatment time. Surface roughness reduces apparently after plasma treatment, as shown in Fig. 3. Plasma treatment could sputter the barriers and make them smooth. Sputtering and stuffing effects are believed to occur due to the reactions or bombardments of energetic radicals and ions during plasma treatment. Resistivity increases with increasing plasma treatment time. It is expected that resistivity of W with plasma treatment would increase because a high-resistivity surface layer is formed and thus the effective thickness of the W film with low resistivity reduces. Resistivity of $W(N_2O)$ barrier is higher than those of the $W(N_2)$ and $W(NH_3)$ barriers. High resistivity may be due to the formation of high-resistance W-O compounds in $W(N_2O)$ barrier, as indicated in XPS analyses. However, the resistivity of $W(N_2O)$ (~24 μΩ cm) barrier is still much lower than that of the reactively sputtered WN film (150 ~ 200 μΩ cm).[8]

Table I summarizes the properties of W, WN and $W(N_2O)$ barriers. Table I also lists properties of sputtered Ta and Ti films in literatures[4,6,16,18] for comparison. The resistivities of sputtered W and $W(N_2O)$ barriers are about 20 and 24 μO cm, respectively. The resistivities are very close and much lower than that of the reactively sputtered WN (150–200 μO cm),[8] Ta (~160 μO cm),[4,16] and Ti (~70 μO cm).[18] Hara *et al.* have reported that the agglomeration and adhesion strength of the copper seed layer, its crystallographic orientation along (111), and the resistivity of the subsequent electro-

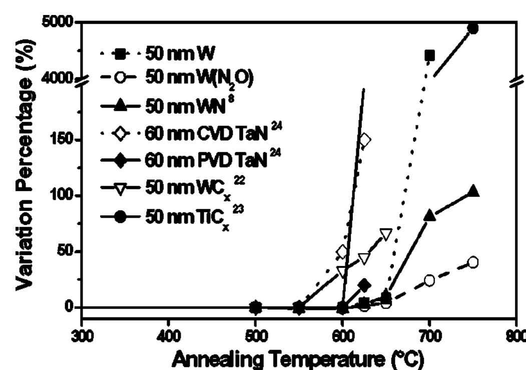

(a)

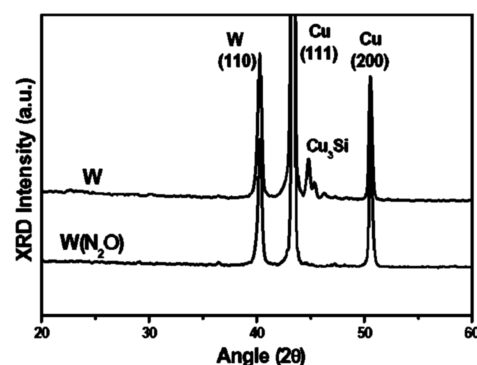

(b)

Figure 4. (a) Variation percentage in sheet resistance of Cu/barrier/Si as a function of annealing temperature. (b) XRD spectra of Cu/W/Si and $Cu/W(N_2O)/Si$ contact systems after annealing at 700°C for 30 min.

plated copper layer, are affected by the stress in the copper seed layer deposited on the barrier layer.[19,20] Electroplating of Cu layer is difficult on seed layers with rough surface. Surface roughness could be reduced from 2.5 to 0.5 nm by N_2O plasma treatment, as listed in Table I. Grain size is calculated from plane-view TEM. The as-deposited W film is columnar grain structure with a grain size of 20–40 nm and grain size of the $W(N_2O)$ barrier is only 2–5 nm. This indicates that nanocrystallization effect would occur due to the reactions and bombardments of energetic radicals and ions during N_2O plasma treatment. Furthermore, it is reported that the impurities (nitrogen or oxygen) in the films are responsible for the intrinsic compressive stress.[21] In this research, the tensile stress decreases from 1.9×10^{10} to 1.4×10^{9} dynes/cm^2 as N_2O plasma treatment is applied to W film, as listed in Table I. N_2O plasma treatment also enhances the adhesion between Cu and $W(N_2O)$ barrier. The adhesion strength of Cu on $W(N_2O)$ barrier (50–58 Mdynes/cm^2) is

Table I. Properties of W, WN, and $W(N_2O)$ diffusion barriers. Properties of sputtered Ta, Ti films are also listed for comparison. Leakage current densities of diodes were measured at a reverse bias of 5 V after annealing at 600°C for 30 min.

	W	$W(N_2O)$	WN[8]	Ta[4,6,16]	Ti[6,18]
Resistivity (μO cm)	~20	~24	150–200	~160	~70
RMS roughness (nm)	2.5	~0.5	1–2	4	3.2–4.2
Grain Size (nm)	20–40	2–5	5–15	20	10–30
Stress (dynes/cm^2)	1.9×10^{10}	1.4×10^{9}	1.5×10^{10}	2.0×10^{10}	3.9×10^{9}
Adhesion	poor	good	poor	poor	fair
Leakage current density (A/cm^2)	$\sim 9.0 \times 10^{-4}$	$\sim 3.0 \times 10^{-9}$	$\sim 8.5 \times 10^{-6}$	2.5×10^{-5}	5.5×10^{-4}

Downloaded on 2014-04-26 to IP 140.113.38.11 address. Redistribution subject to ECS terms of use (see ecsdl.org/site/terms_use) unless CC License in place (see abstract).

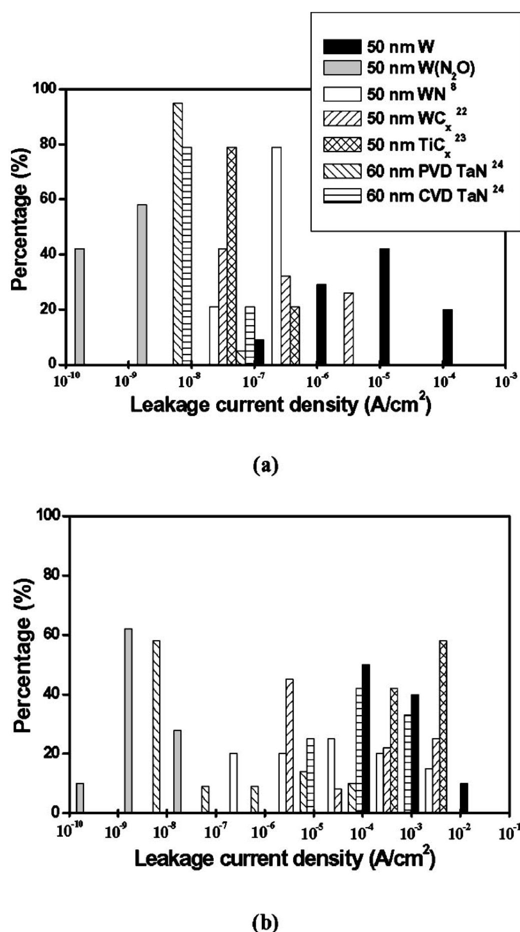

Figure 5. Statistical distributions of leakage current densities of copper contacted n^+-p junction diodes with various diffusion barriers after annealing at (a) 500 and (b) 600°C for 30 min.

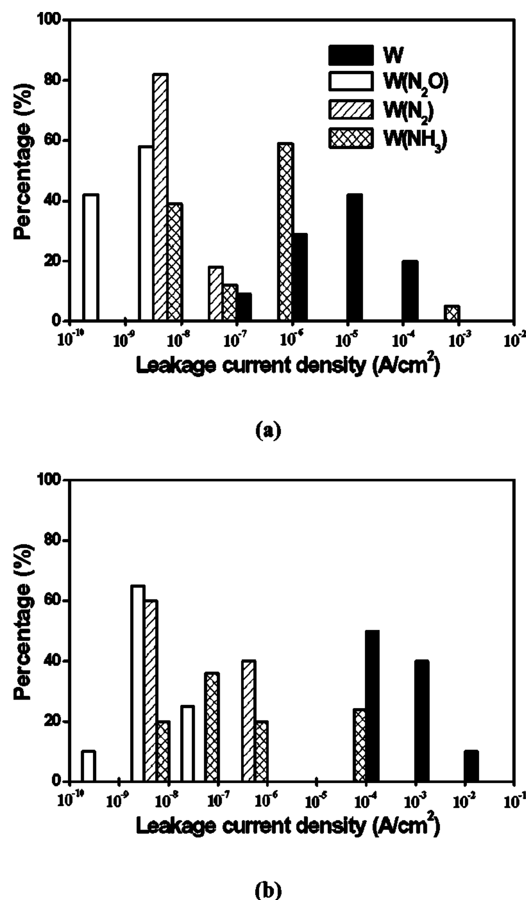

Figure 6. Statistical distributions of leakage current densities of copper contacted n^+-p junction diodes with various plasma-treated W diffusion barriers after annealing at (a) 500 and (b) 600°C for 30 min.

better than untreated W (30–35 Mdynes/cm^2) and other barriers such as Ta and Ti.[6] It is suggested that O or N species on the barrier surface can react with Cu to form more stable interface and thus promote adhesion after N_2O plasma treatment.

Figure 4a shows the variation percentage of the Cu/barrier/Si system after furnace annealing at various temperatures. The variation in sheet resistance is defined as the ratio of $(R - R_0)$ to R_0, in which R_0 and R denote the sheet resistance of as-deposited and annealed samples. The results reflect the interactions between Cu and Si indirectly. Resistance increases rapidly at certain temperature because of failure of the diffusion layer and formation of compounds. Sheet resistance of Cu/W(N_2O)/Si increases slightly even after annealing at 750°C. However, sheet resistances of samples with other barriers (W, WN,[8] WC_x,[22] TiC_x,[23] and TaN[24]) sharply increase after annealing at 600–700°C, indicating that a considerable amount of Cu has already diffused through the barrier layers and resulted in Cu_3Si compounds, and thus strongly deteriorated the conductivity of the contact system. XRD was further used to detect the structural change in the annealed samples. Figure 4b shows XRD patterns of Cu/W/Si and Cu/W(N_2O)/Si systems after annealing at 700°C for 30 min. Peaks of Cu_3Si compounds are observed for W barrier and the resulting XRD pattern is consistent with variation in sheet resistance. There is no Cu_3Si peak in W(N_2O) barrier system, indicating that W(N_2O) has an excellent barrier performance. It is noted that there is no Cu-W compound in the XRD spectra, and similar results are found for WN barriers.[8] The failure of W and WN barriers is attributed that Cu atoms diffuse through defects and grain boundaries of the barrier without reacting with the WN and W film. Failure temperature (variation percentage $> 50\%$) of W(N_2O) barrier is higher than 750°C and superiors to sputtered WC_x(~650°C),[22] TiC_x(~625°C),[23] and TaN(~650°C)[24] barriers.

Barrier performance is also evaluated by the leakage current density of the junction diode. Figure 5 illustrates the statistical distributions of leakage current densities of Cu/barrier/n^+-p junction diodes measured at reverse bias of 5 V after annealing at 500 and 600°C. The leakage current densities of all diodes are below 10^{-8} A/cm^2 before annealing. Most diodes with sputtered W, WN,[8] WC_x,[22] and TiC_x[23] barriers have leakage current densities higher than 1×10^{-7} A/cm^2 after annealing at 500°C for 30 min. Diodes with W(N_2O) barriers retain leakage current densities less than 10^{-8} A/cm^2 after annealing at 500°C. Moreover, most diodes with W(N_2O) barriers retain leakage current densities less than 10^{-8} A/cm^2 even after annealing at 600°C. W(N_2O) show an excellent barrier capability against Cu diffusion compared to W, WN,[8] WC_x,[22] TiC_x,[23] and TaN,[24] as shown in Fig. 5.

Although barrier performance of the W film is significantly improved by N_2O plasma treatment, similar plasma treatments, *e.g.*, N_2 plasma treatment, had been proposed to enhance barrier performance in previous researches.[15,16] W barriers are also treated by N_2 or NH_3 plasma for comparison in the work. Figure 6 exhibits statistical distributions of leakage current densities of Cu/W(N_2O)/n^+-p, Cu/W(N_2)/n^+-p and Cu/W(NH_3)/n^+-p diodes after annealing at 500 and 600°C. All W(N_2O), W(N_2), and W(NH_3) show an enhanced barrier performance compared to untreated W. Moreover, N_2O plasma treatment has a better barrier improvement than N_2

Downloaded on 2014-04-26 to IP 140.113.38.11 address. Redistribution subject to ECS terms of use (see ecsdl.org/site/terms_use) unless CC License in place (see abstract).

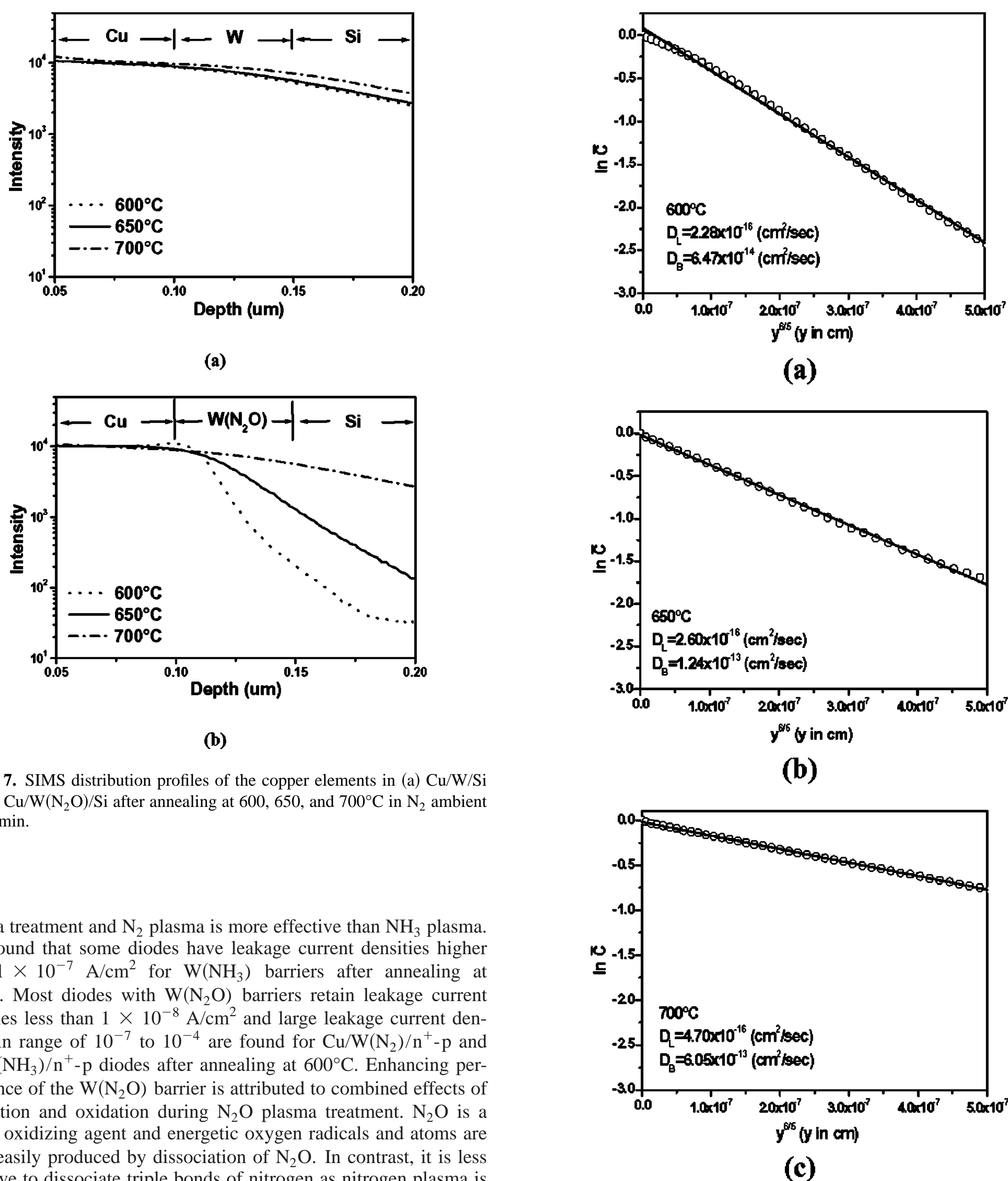

Figure 7. SIMS distribution profiles of the copper elements in (a) Cu/W/Si and (b) $Cu/W(N_2O)/Si$ after annealing at 600, 650, and 700°C in N_2 ambient for 30 min.

Figure 8. Penetration plots for Cu diffusion into W films at various temperatures of (a) 600, (b) 650, and (c) 700°C. The solid curve is the fitting curve.

plasma treatment and N_2 plasma is more effective than NH_3 plasma. It is found that some diodes have leakage current densities higher than 1×10^{-7} A/cm^2 for $W(NH_3)$ barriers after annealing at 500°C. Most diodes with $W(N_2O)$ barriers retain leakage current densities less than 1×10^{-8} A/cm^2 and large leakage current densities in range of 10^{-7} to 10^{-4} are found for $Cu/W(N_2)/n^+$-p and $Cu/W(NH_3)/n^+$-p diodes after annealing at 600°C. Enhancing performance of the $W(N_2O)$ barrier is attributed to combined effects of nitridation and oxidation during N_2O plasma treatment. N_2O is a strong oxidizing agent and energetic oxygen radicals and atoms are more easily produced by dissociation of N_2O. In contrast, it is less effective to dissociate triple bonds of nitrogen as nitrogen plasma is used to post-treat W barrier. The bond strengths of N-O and N-N are 630.57 and 945.33 kJ/mol. Energetic oxygen radicals and atoms are helpful in formation of an oxygen stuffed layer on the columnar-grained W barrier. It will act as a more efficient barrier against the Cu diffusion. N_2 plasma treatment does not induce oxygen stuffed layer on surface of the W barrier and nitrogen radicals and atoms are limited for nitridation and stuffing compared to N_2O plasma treatment. Bond strength of N-H is 339 kJ/mol for NH_3 plasma treatment. Although nitridation is expected to occur greatly, no plasma oxidation on W surface occurs and lots of atomic hydrogen will diffuse into the grain boundaries of W due to effective dissociation of NH_3. Hydrogen will out-diffuse from grain boundaries of plasma-treated W after annealing at a certain temperature, lead to defect sites or carrier trapping sites, and hence, decrease its resistance to copper penetration.

Barrier capabilities are further investigated by evaluating Cu diffusion in W and $W(N_2O)$ barriers. The diffusion of Cu in the temperature range of 600–700°C is evaluated by SIMS and the penetration depth profiles of specimens are indicated in Fig. 7. Relatively low Cu penetration into the $W(N_2O)$ barrier is detected compared to sputtered W barrier. Because the mixing enthalpy of Cu solute in W is large (8.0×10^4 j/mol), Cu atoms do not intermix with W at high temperature.[25,26] As far as we know, it is relatively difficult for Cu penetration into W barrier by lattice diffusion. However, the diffusion coefficients of Cu in grain boundaries of W barrier are still

Downloaded on 2014-04-26 to IP 140.113.38.11 address. Redistribution subject to ECS terms of use (see ecsdl.org/site/terms_use) unless CC License in place (see abstract).

Table II. Summary of the values of diffusivities, pre-exponential factors, and activation energies for Cu diffusion in W films at various annealing temperatures.

Sample	T (°C)	D_L (cm²/s)	D_B (cm²/s)	D_{L0} (cm²/s)	Q_L (eV)	D_{B0} (cm²/s)
W	600	2.28×10^{-16}	6.47×10^{-14}	1.83×10^{-13}	0.508	1.28×10^{-4}
	650	2.60×10^{-16}	1.24×10^{-13}			
	700	4.70×10^{-16}	6.05×10^{-13}			

unknown, though the rough estimation has been discussed,[27] and the results are still needed to be further discussed.

Whipple had given formulas for the concentration in a semi-infinite region of low diffusion coefficient bisected by a thin well-diffusing slab. Because our source condition is close to infinite one, the Whipple's solution is used for profile analysis.[11] The key result of Whipple's solution is

$$D_B\delta = 0.661\left(-\frac{\partial \ln(\bar{C})}{\partial y^{6/5}}\right)^{-5/3}\left(\frac{4D_L}{t}\right)^{1/2} \quad [1]$$

where $\bar{C} = C/C_s$, C represents the concentration in a section at a depth y μm from the original surface, C_s is the surface concentration, t is the annealing time, and d is the grain boundary width. D_L and D_B present the diffusion coefficients in the lattice and the grain boundary. Figure 8 displays the concentration profiles obtained from diffusion of Cu in W barriers at various temperatures in the standard coordinates $\ln \bar{C}$ *vs.* $y^{6/5}$. Based on Eq. 1 and provided that D_L is known, δD_B can be determined by measuring the slope from the linear region in the $\ln \bar{C}$ *vs.* $y^{6/5}$ plots. The value of D_L can be found from the initial part of the concentration profile. Under the assumptions of a semi-infinite system and constant source at the surface, the boundary conditions applied to solve Fick's diffusion equation are

$$C = C_s, \quad y < 0, \quad t = 0 \quad [2]$$

$$C = 0, \quad y > 0, \quad t = 0 \quad [3]$$

An error function solution can be expressed by the equation

$$C(y, t) = C_s \,\mathrm{erfc}\left(\frac{y}{2\sqrt{D_L t}}\right) \quad [4]$$

where the error function was fitted to the initial part of the concentration profiles and extrapolated to zero thickness $y = 0$ in the case of subtracting the grain boundary contribution. The results are shown in Table II, and the derived value of D_L was used to calculate δD_B. To obtain a value D_B, a grain boundary width must be assumed, it is reasonable to assume a width of about two atom layers, $\delta = 5 \times 10^{-8}$ cm.[28,29]

Based on the numerical calculation, a satisfactory fitting to the experimental depth profile can be obtained.[10] The temperature dependence of the grain boundary diffusivity in W barrier can be expressed by the Arrhenius relation of $D_B = D_{B0}\exp(-Q_B/kT)$, as plotted in Fig. 9, where D_{B0} is the pre-exponential factor, Q_B is the activation energy for grain boundary diffusion, k is the Boltzmann constant, and T is annealing temperature. Also, the temperature dependence of the lattice diffusivity in W barrier can be expressed by the Arrhenius relation of $D_L = D_{L0}\exp(-Q_L/kT)$, where D_{L0} and Q_L are pre-exponential factor and activation energy for lattice diffusion. The dependency is plotted in Fig. 10. The values of diffusivities, pre-exponential factors, and activation energies are summarized in Table II. The D values of Cu in sputtered W films are smaller than those in CVD-W films, but the magnitudes are in the same order. In addition, the activation energy of Cu diffusion in sputtered W films is somewhat larger than that in CVD-W films.[27,30]

Similar numerical analysis can be applied to evaluate the effects of Cu diffusion in $W(N_2O)$ barriers. As mentioned previously, N_2O plasma treatment causes an amorphous surface layer upon the W film. This is the case of a semi-infinite medium which has a skin or surface layer $W(N_2O)_1$ having diffusion properties different from those of the rest of the medium $W(N_2O)_2$. The subscripts 1 and 2 denote the amorphous surface layer and the rest in the $W(N_2O)$ barrier. Thus, suppose in the semi-infinite region $-h < y' < \infty$, the lattice diffusion coefficient is D_{L1} in the region $-h < y' < 0$, and the concentration is denoted by C_1 there, while the corresponding quantities in $y' > 0$ are D_{L2} and C_2. Assume the conditions at the interface to be $C_1 = C_2$, $y' = 0$ and $D_{L1}\partial C_1/\partial y' = D_{L2}\partial C_2/\partial y'$, $y' = 0$ the solution to the problem of zero initial concentration and the surface $y' = -h$ maintained at constant concentration C_0 is given as[12]

$$C_1 = C_0 \sum_{n=0}^{\infty} \alpha^n \left\{ \mathrm{erfc}\frac{(2n+1)h + y'}{2\sqrt{D_{L1}t}} - \alpha\, \mathrm{erfc}\frac{(2n+1)h - y'}{2\sqrt{D_{L1}t}} \right\} \quad [5]$$

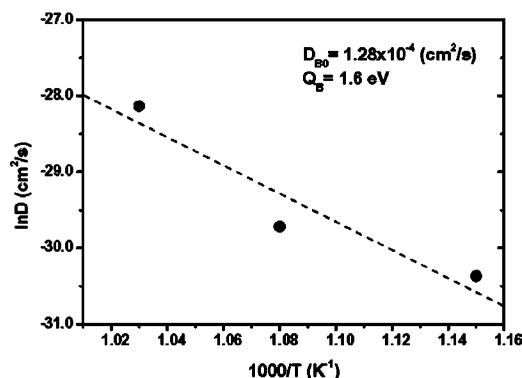

Figure 9. The Arrhenius plot of the grain boundary diffusivity D_B for Cu diffusion in W films.

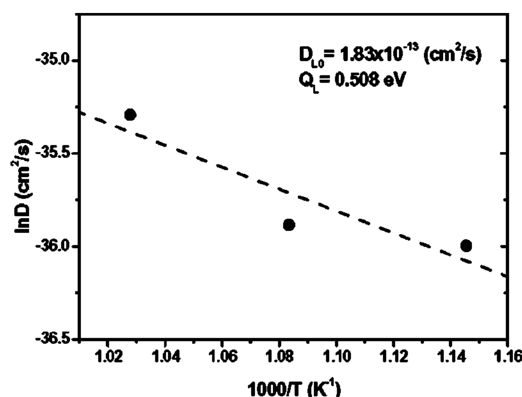

Figure 10. The Arrhenius plot of the lattice diffusivity D_L for Cu diffusion in W films.

Downloaded on 2014-04-26 to IP 140.113.38.11 address. Redistribution subject to ECS terms of use (see ecsdl.org/site/terms_use) unless CC License in place (see abstract).

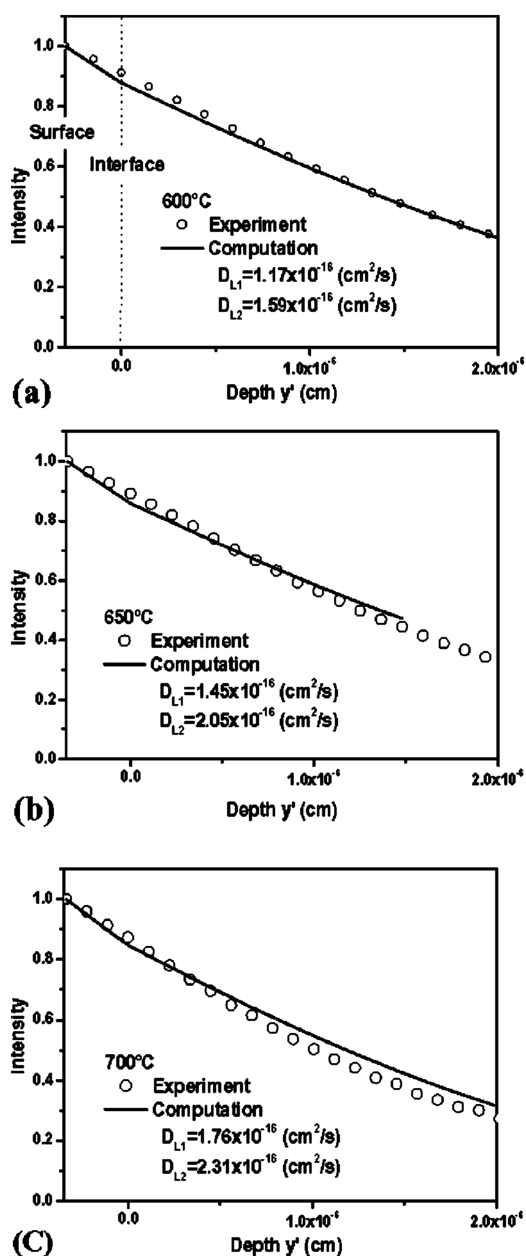

Figure 11. Penetration plots for Cu diffusion into $W(N_2O)$ films at various temperatures of (a) 600, (b) 650, and (c) 700°C. The solid curve is the profile calculated from Eq. 5 and 6.

$$C_2 = \frac{2kC_0}{k+1}\sum_{n=0}^{\infty}\alpha^n \operatorname{erfc}\frac{(2n+1)h + ky'}{2\sqrt{D_{L1}t}} \qquad [6]$$

where $k = \sqrt{D_{L1}/D_{L2}}$, $\alpha = (1-k)/(1+k)$

The thickness h of the surface layer $W(N_2O)_1$ is about 3 nm from high-resolution TEM micrograph. Both diffusion coefficients can be obtained by numerical calculation. The values of D_{L1} and D_{L2} can be roughly estimated from fitting of experimental concentration profiles using an error function solution such as that in Eq. 4. The estimated values are used as the initial guess of D_{L1} and D_{L2} and further substituted into the Eq. 5 and 6 to obtain concentrations C_1 and C_2, respectively. To quickly obtain the numerical convergence, the high order terms are neglected in the Eq. 5 and 6 during the calculation. It is found that the calculated error is smaller than 10^{-4} as $n = 4$. The asymptotic solutions of lattice diffusion coefficients can be obtained by steep-descent method and fitting of the experimental concentration profile. Figure 11 shows experimental and calculated concentration profiles. The derived values of D_{L1} and D_{L2} are listed in Table III.

Similarly, grain boundary diffusion coefficients D_{B2} in $W(N_2O)_2$ region can be determined from the derived lattice diffusion coefficient D_{L2} and the slope in $\ln \bar{C}$ *vs.* $y'^{6/5}$ plots. Figure 12 displays experimental concentration profiles for Cu diffusion in $W(N_2O)$ barriers at various annealing temperatures in the standard coordinates $\ln \bar{C}$ *vs.* $y'^{6/5}$. The derived grain boundary diffusion coefficients D_{B2} are listed in Table III. Table III summaries the values of diffusion coefficients and pre-exponential factors for Cu diffusion in $W(N_2O)$ barriers. Other barrier materials in literatures are also listed for comparison.[27,30,31] The $W(N_2O)$ barrier shows small lattice diffusion coefficients compared to W_2N, W, and TiB_2 barriers. The variation of D_{L2} with temperature is slight for the $W(N_2O)$ barrier, indicating that the $W(N_2O)$ barrier has better thermal stability.

One significant finding in the present study is that some atomic nitrogen and oxygen will react with W, segregate at grain boundaries of W film as impurities, and act as a stuffing agent to block fast diffusion path during N_2O plasma treatment. Nitrogen addition will stuff the grain boundaries of W and nitrify tungsten to form tungsten nitride, as shown in XPS analyses of Fig. 1c. Similar nitridation effect had been reported by Hara *et al.*[32] A TiN barrier was formed at the surface of the Ti layer in high-pressure ammonium ambient. Figure 13 shows cross sections of the interfacial structures of Cu/W/Si and Cu/$W(N_2O)$/Si samples before and after annealing. The as-deposited W barrier has a columnar grain structure as shown in Fig. 13a. The failure of W barrier is attributed to the Cu diffusion through the columnar W to form Cu_3Si after annealing at 700°C for 30 min. Grain boundary diffusion coefficients are $6.5 \times 10^{-14} \sim 6.1 \times 10^{-13}$ cm^2/s using Whipple analysis of grain boundary

Table III. Summary of the values of diffusivities, and pre-exponential factors for Cu diffusion in $W(N_2O)$ films and at various annealing temperatures. Other barrier materials are also listed for comparison.

		D_L (cm^2/s)		D_B (cm^2/s)	D_{L0} (cm^2/s)		
Sample	T (°C)	D_{L1}	D_{L2}	D_{B2}	$D_{L0,1}$	$D_{L0,2}$	D_{B0} (cm^2/s)
$W(N_2O)$	600	1.17×10^{-16}	1.58×10^{-16}	4.07×10^{-14}	6.12×10^{-15}	6.43×10^{-15}	9.28×10^{-13}
	650	1.45×10^{-16}	2.04×10^{-16}	5.37×10^{-14}			
	700	1.76×10^{-16}	2.31×10^{-16}	5.57×10^{-14}			
W_2N[27]	600	1.15×10^{-16}			7.00×10^{-11}		
	700	4.52×10^{-16}					
W[30]	600	2.4×10^{-16}			1.11×10^{-13}		
	700	4.5×10^{-16}					
TiB_2[31]	500	1.4×10^{-15}					
	600	2.0×10^{-15}					
	700	5.3×10^{-15}					
	800	5.0×10^{-14}					

Downloaded on 2014-04-26 to IP 140.113.38.11 address. Redistribution subject to ECS terms of use (see ecsdl.org/site/terms_use) unless CC License in place (see abstract).

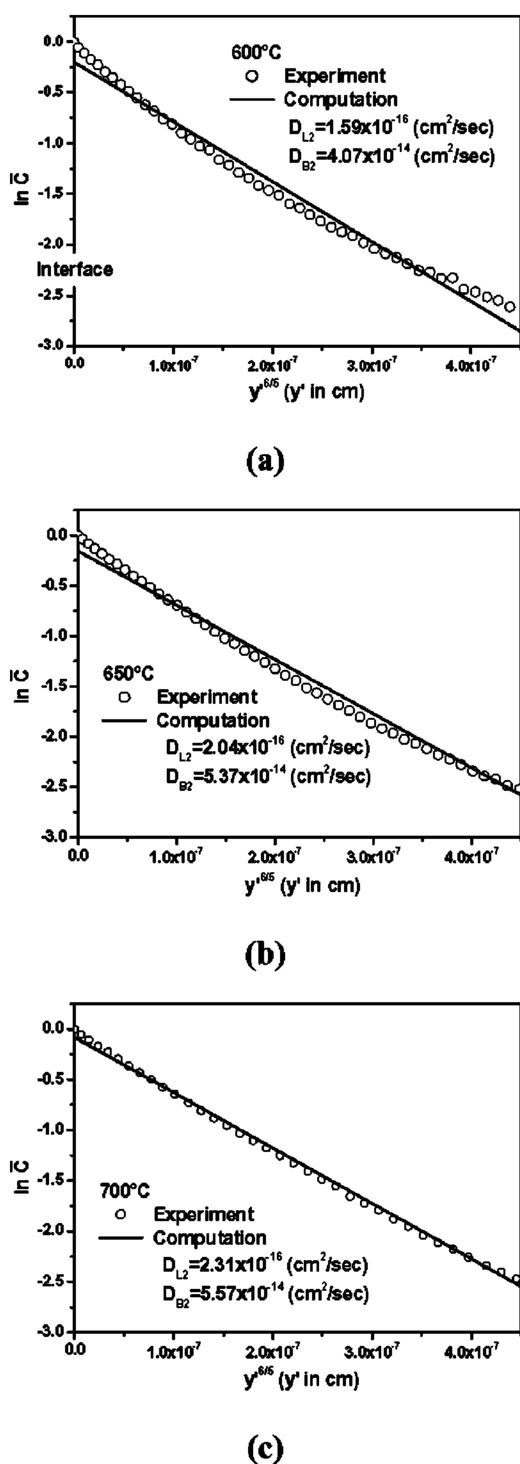

Figure 12. Penetration plots for Cu diffusion into $W(N_2O)$ films at various temperatures of (a) 600, (b) 650, and (c) 700°C. The solid curve is the fitting curve.

diffusion. The barrier capability of the W film against Cu diffusion can be improved by N_2O plasma treatment. An oxidation and nitridation layer with nanostructured grains is formed on the surface of the stuffed W barrier, as shown in Fig. 13b. Relatively low diffusion coefficients are found. No Cu silicide compound is observed for $Cu/W(N_2O)/Si$ sample after annealing at 700°C for 30 min because nanostructured and stuffed barrier can effectively impede Cu diffusion.

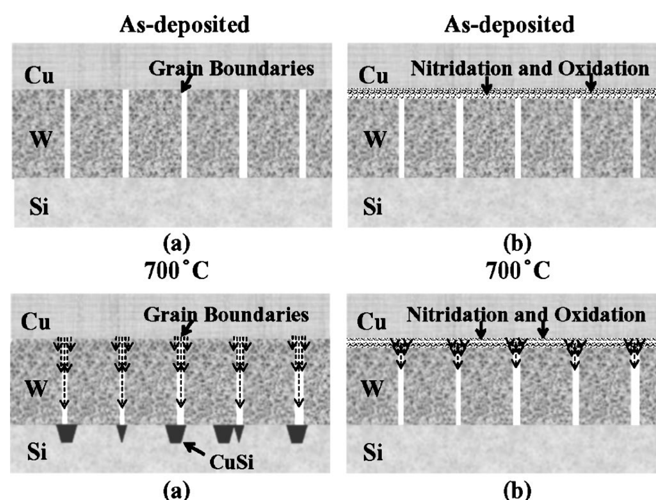

Figure 13. Schematic illustrations of the microstructures of (a) Cu/W/Si and (b) $Cu/W(N_2O)/Si$ samples before and after annealing.

Conclusion

The effectiveness of $W(N_2O)$ films as diffusion barriers between Cu and Si has been investigated. $W(N_2O)$ films, which have amorphous and nano-grained surface layers, show high thermal stability, low resistivity, low surface roughness, low tensile stress, and better adhesion with Cu. $W(N_2O)$ barriers show excellent barrier capabilities against Cu diffusion. $Cu/W(N_2O)/n^+$-p junction diodes retain leakage current densities less than 10^{-8} A/cm^2 even after annealing at 600°C. Copper diffusion in W and $W(N_2O)$ barriers is further analyzed using the Whipple analysis of grain boundary diffusion and Fick's diffusion law. Both lattice and grain boundary diffusivities of Cu diffusion in W and $W(N_2O)$ barriers are extracted from the Cu concentration profiles after annealing the samples at 600–700°C. Grain boundary diffusion coefficients of Cu in sputtered W films are $6.5 \times 10^{-14} \sim 6.1 \times 10^{-13}$ cm^2/s. Relatively low diffusion coefficients are found in $W(N_2O)$ barriers because oxidation and nitridation layers with nano grains are formed at the surface of the stuffed W barriers after N_2O plasma treatments.

Acknowledgments

The work reported was financially supported by the National Science Council of the Republic of China under contract no. NSC 92-2215-E-492-002 and supported, in part, by the Ministry of Economic Affairs of the Republic of China under contract no. 92-EC-17-A-08-S1-0003. Technical support from the National Nano Device Laboratories is greatly acknowledged.

The National Nano Device Laboratories assisted in meeting the publication costs of this article.

References

1. S. D. Brotherton, J. R. Ayres, A. Gill, H. W. V. Kesteren, and F. J. A. M. Greidanus, *J. Appl. Phys.*, **62**, 1826 (1987).
2. J. M. Shieh, K. C. Tsai, and B. T. Dai, *Appl. Phys. Lett.*, **82**, 1914 (2003).
3. S. M. Rossnagel, I. C. Noyan, and C. Cabral, Jr., *J. Vac. Sci. Technol. B*, **20**, 2047 (2002).
4. W. L. Yang, W. F. Wu, D. G. Lin, C. C. Wu, and K. L. Ou, *Solid-State Electron.*, **45**, 149 (2001).
5. K. H. Min, K. C. Chun, and K. B. Kim, *J. Vac. Sci. Technol. B*, **14**, 3263 (1996).
6. H. Ono, T. Nakano, and T. Ohta, *Appl. Phys. Lett.*, **64**, 1511 (1994).
7. S. Wong, C. Ryu, H. Lee, and K. Kwon, *Mater. Res. Soc. Symp. Proc.*, **514**, 75 (1998).
8. K. C. Tsai, W. F. Wu, J. C. Chen, T. J. Pan, and C. G. Chao, *J. Vac. Sci. Technol. B*, **22**, 993 (2004).
9. W. F. Wu, K. C. Tsai, C. G. Chao, C. F. Huang, S. T. Wu, Y. L. Chin, and B. S. Chiou, in *Proceedings of the 17th International VLSI Multilevel Interconnection Conference*, IEEE, p. 490 (2000).
10. J. C. Lin and C. Lee, *J. Electrochem. Soc.*, **146**, 3466 (1999).
11. R. T. P. Whipple, *Philos. Mag.*, **45**, 1225 (1954).

Downloaded on 2014-04-26 to IP 140.113.38.11 address. Redistribution subject to ECS terms of use (see ecsdl.org/site/terms_use) unless CC License in place (see abstract).

12. J. Crank, *The Mathematics of Diffusion*, Clarendon Press, Oxford (1975).
13. J. F. Moulder, W. F. Stickle, P. E. Sobol, and K. D. Bomben, *Handbook of X-Ray Photoelectron Spectroscopy*, Physical Electronics, Inc., Eden Prairie, MN (1995).
14. T. Nakajima, K. Watanabe, and N. Watanabe, *J. Electrochem. Soc.,* **134**, 3175 (1987).
15. K. M. Chang, T. H. Yeh, I. C. Deng, and C. W. Shih, *J. Appl. Phys.,* **82**, 1469 (1997).
16. W. F. Wu, K. L. Ou, C. P. Chou, and C. C. Wu, *J. Electrochem. Soc.,* **150**, G83 (2003).
17. D. J. Kim, Y. T. Kim, and J. W. Park, *J. Appl. Phys.,* **82**, 4847 (1997).
18. M. E. Day, M. Delfino, J. A. Fair, and W. Tsai, *Thin Solid Films,* **254**, 285 (1995).
19. T. Hara, Y. Yoshida, and H. Toida, *Electrochem. Solid-State Lett.,* **5**, G36 (2002).
20. T. Hara, Y. Shimura, and H. Toida, *Electrochem. Solid-State Lett.,* **6**, C97 (2003).
21. H. Windischmann, *J. Vac. Sci. Technol. A,* **9**, 2459 (1991).
22. S. J. Wang, H. Y. Tsai, S. C. Sun, and M. H. Shiao, *J. Electrochem. Soc.,* **148**, G500 (2001).
23. S. J. Wang, H. Y. Tsai, S. C. Sun, and M. H. Shiao, *J. Electrochem. Soc.,* **148**, C563 (2001).
24. M. H. Tsai, S. C. Sun, C. E. Tsai, S. H. Chuang, and H. T. Chiu, *J. Appl. Phys.,* **79**, 6932 (1996).
25. M. E. Glicksman, *Diffusion in Solid*, p. 207, Wiley Interscience, New York (2000).
26. F. R. de Boer, R. Boom, W. C. M. Mattens, A. R. Miedema, and A. K. Niessen, *Cohesion in Metals, Transition Metal Alloys*, North-Holland, Amsterdam (1988).
27. M. Uekubo, T. Oku, K. Nii, M. Murakami, K. Takahiro, S. Yamaguchi, T. Nakano, and T. Ohta, *Thin Solid Films,* **286**, 170 (1996).
28. D. Gupta and T. T. C. Tsui, *Appl. Phys. Lett.,* **17**, 294 (1970).
29. J. C. Fisher, *J. Appl. Phys.,* **22**, 74 (1951).
30. K. Vieregge and D. Gupta, *Tungsten and Tungsten Alloys-Recent Advances*, p. 231, The Minerals, Metals and Materials Society (1991).
31. J. Pelleg and G. Sade, *J. Appl. Phys.,* **91**, 6099 (2002).
32. T. Hara, K. Tani, and K. Inoue, *Appl. Phys. Lett.,* **57**, 1660 (1990).

Downloaded on 2014-04-26 to IP 140.113.38.11 address. Redistribution subject to ECS terms of use (see ecsdl.org/site/terms_use) unless CC License in place (see abstract).